Journal of Nuclear Materials 479 (2016) 447–454

Contents lists available at ScienceDirect

Journal of Nuclear Materials

journal homepage: www.elsevier.com/locate/jnucmat

Microhardness and Young's modulus of high burn-up UO_2 fuel

F. Cappia [a, b], D. Pizzocri [a, c], M. Marchetti [a, d], A. Schubert [a], P. Van Uffelen [a], L. Luzzi [c], D. Papaioannou [a], R. Macián-Juan [b], V.V. Rondinella [a, *]

[a] European Commission, Joint Research Centre, Institute for Transuranium Elements, P.O. Box 2340, 76125, Karlsruhe, Germany
[b] Technische Universität München, Faculty of Mechanical Engineering, Department of Nuclear Engineering, D-85748, Garching bei München, Germany
[c] Politecnico di Milano, Department of Energy, Nuclear Engineering Division, 20156, Milano, Italy
[d] Université Montpellier 2, Institut d'Electronique du Sud UMR CNRS 5214, 34095, Montpellier, France

HIGHLIGHTS

- Vickers microhardness and Young's modulus data of high burnup fuels are presented.
- The data are compared to fuel performance codes' correlations.
- A burn-up dependent factor is introduced for the Young's modulus of irradiated fuel.
- The modification extends ranges of experimental validation of the code correlation.
- The new burn-up dependent factor has limited effect on integral fuel performance.

ARTICLE INFO

Article history:
Received 15 February 2016
Received in revised form
5 July 2016
Accepted 6 July 2016
Available online 19 July 2016

Keywords:
High burn-up UO_2 fuel
Vickers microhardness
Young's modulus
TRANSURANUS

ABSTRACT

Vickers microhardness ($HV_{0.1}$) and Young's modulus (E) measurements of LWR UO_2 fuel at burn-up $\geq$60 GWd/tHM are presented. Their ratio $HV_{0.1}/E$ was found constant in the range 60–110 GWd/tHM. From the ratio and the microhardness values vs porosity, the Young's modulus dependence on porosity was derived and extended to the full radial profile, including the high burn-up structure (HBS). The dependence is well represented by a linear correlation. The data were compared to fuel performance codes correlations. A burn-up dependent factor was introduced in the Young's modulus expression. The modifications extend the experimental validation range of the TRANSURANUS correlation from unirradiated to irradiated UO_2 and up to 20% porosity.

First simulations of LWR fuel rod irradiations were performed in order to illustrate the impact on fuel performance. In the specific cases selected, the simulations suggest a limited effect of the Young's modulus decrease due to burn-up on integral fuel performance.

1. Introduction

When operating fuel at high burn-up, a possible matter of concern is the enhanced pellet-cladding interaction (PCI) following the progressive closure of the gap [1]. Despite its beneficial effect on the heat transfer between fuel and cladding, the PCI can shorten the cladding lifetime due to the stresses induced by the fuel onto the cladding paired with accumulation of chemically aggressive volatile fission products [2]. Moreover, at high burn-up the fuel swelling is increased by the steep build-up of porosity associated with the high burn-up structure (HBS) formation. Ultimately, the increased fuel gaseous swelling can severely impact the fuel-cladding contact pressure [3].

Experimental data relating the mechanical properties of irradiated UO_2 to its local microstructure are of practical importance to ameliorate the understanding of how high burn-up fuel properties can affect the PCI and to support the development of predictive models in fuel performance codes. Among several structural factors that affect the fuel mechanical properties (e.g., accumulation of radiation damage, porosity, grain size, local deviations from stoichiometry), the porosity is thought to play a major role while reducing the load-bearing area, especially in the HBS [4]. The highly heterogeneous character of the irradiated fuel microstructure along the pellet radius makes the experimental investigations difficult. The traditional mechanical testing methods are either not

* Corresponding author.
E-mail address: Vincenzo.RONDINELLA@ec.europa.eu (V.V. Rondinella).

http://dx.doi.org/10.1016/j.jnucmat.2016.07.015

applicable to irradiated fuel or can provide data that reflects only averaged properties of the pellet because of spatial resolution limitations [4]. Considerable improvement has been achieved through the application of micro-gauge techniques like high-frequency acoustic microscopy [5] and microhardness [4], which offer relatively high spatial resolution. Using acoustic microscopy, Laux et al. [5] studied the dependence of the fuel Young's modulus on burn-up, showing a global decrease of 20–25% up to ≈100 GWd/tHM. Using Vickers microindentation, Spino et al. [4] studied the porosity dependence of the irradiated fuel microhardness revealing the softening of the fuel as a result of the porosity increase at the radial periphery of the pellet, in particular in the HBS.

The microhardness data are not directly used in fuel performance codes, whereas the fuel Young's modulus is employed. Its relationship with porosity is of particular interest. The correlations of the fuel Young's modulus with porosity implemented in the codes generally rely on data from non-irradiated UO_2 [6–8]. Typically, these expressions are linear correlations whose slope reflects the geometry of the lenticular pores in sintered solids [9]. As the porosity in the HBS is composed of spherical cavities [10], direct application of such relationships to HBS may be questionable.

In this context, the scope of this work was twofold. Firstly, we aimed at experimentally investigating the relationship between the Young's modulus and the local porosity of high burn-up UO_2 fuel, especially in the HBS. The relationship between Young's modulus and local porosity in the HBS could not be directly investigated so far. This is mainly due to the limited applicability of the current experimental set-up (i.e., a scanning acoustic microscope adapted for use in hot cells) to the relevant pellet rim regions, especially where the increase of porosity is the highest. The HBS thickness is generally less than the currently accessible acoustic microscope spatial resolution; moreover, the cladding presence interferes with the signal. The aforementioned experimental limitations were tackled combining the results of Vickers microindentation and acoustic microscopy. An experimental campaign was conducted to assess the relationship between Vickers microhardness and local porosity measured using Scanning Electron Microscopy (SEM). At the same time, an empirical relationship between the local Vickers microhardness ($HV_{0.1}$) and Young's modulus (E) was studied, namely their ratio ($HV_{0.1}/E$). As $HV_{0.1}/E$ was determined to be constant, it was possible to obtain an estimation of the Young's modulus as a function of local porosity. This allowed direct comparison with correlations obtained from unirradiated UO_2, and implementation of the experimental relationship of Young's modulus vs. porosity in the fuel performance code TRANSURANUS V1M1J14, in order to extend its reliance on irradiated UO_2 fuel data. Secondly, the impact of mechanical properties of high burn-up fuel on integral fuel performance was studied by performing preliminary TRANSURANUS simulations.

The paper is organised as follows: Sections 2 and 3 describe the experimental work conducted on the mechanical properties of high burn-up fuel and the comparison of the Young's modulus vs. porosity correlation derived from irradiated fuel measurements with the TRANSURANUS correlation and other correlations available in the open literature. In Section 4, preliminary results of the TRANSURANUS simulations of two high burn-up experimental fuel rods are reported. Finally, conclusions and outlook considerations are drawn.

2. Experimental

2.1. Fuel samples

The measurements were carried out both on commercial fuel samples irradiated in Pressurized Water Reactors and on special irradiation disc samples. The commercial samples had an initial enrichment of 3.5–3.95 wt% ^{235}U, a density of 95–96%TD and were irradiated up to average burn-up of 67 GWd/tHM and 100 GWd/tHM. The experimental discs were part of the Nuclear Fuel Industry Research (NFIR) program [11]. The discs were irradiated in the Halden reactor up to 103 GWd/tHM, had an initial enrichment of ≈20 wt% ^{235}U and a density of 95–96.5%TD. The special configuration and controlled conditions of the Halden disc irradiation (i.e., isothermal irradiation, end of irradiation by scram to “freeze” the actual fuel configuration at the irradiation temperature) allowed obtaining discs with uniform burn-up and with morphology and structure representative of fuel under irradiation.

2.2. Vickers microindentation

The samples were first carefully ground and polished in several steps using diamond suspensions with particle size from 12 μm to 1 μm . A Micro-Duromat 4000E microhardness Vickers tester, incorporated in a shielded LEICA Telatom 3 optical microscope, was used. The tests were performed at room temperature under N_2 atmosphere [4]. The microindentations were performed according to the standard for Vickers indentation for advanced ceramics ASTM C1327 [12]. A 0.98 N load was employed, with a loading rate of $9.8 \cdot 10^{-3}$ N/s and a hold time at the maximum load of 12 s. A minimum of 5 indentations was performed at each of the different locations selected. The diagonals of the imprints were measured from images acquired with the optical microscope at magnification 1500x. The Vickers microhardness $HV_{0.1}$ (GPa) was computed using the following relation [12],

$$HV_{0.1} = 0.0018544 \frac{P}{d^2} \tag{1}$$

where P (N) is the applied maximum load and d (mm) is the average length of the two diagonals of the indentation.

2.3. Scanning acoustic microscopy

A scanning acoustic microscope has been developed and adapted to measure the elastic moduli (i.e., Young's modulus E and shear modulus G) of irradiated UO_2 fuel [5,13]. The Young's modulus E can be calculated from the following relationship [5],

$$E \approx 3\rho v_R^2 \tag{2}$$

where E (Pa) is the Young's modulus, ρ (kg m^{-3}) is the sample local density, and v_R (m s^{-1}) is the measured Rayleigh wave velocity. The sample local density can be empirically related to the Rayleigh wave velocity using the following equation [14].

$$\rho = 3.3 v_R + 2.0495 \cdot 10^3 \tag{3}$$

where all the symbols have the same meaning as in Eq. (2). Combining Eq. (2) and Eq. (3), the Young's modulus can be calculated from the single measurement of v_R.

2.4. Scanning electron microscopy and quantitative image analysis (QIA)

The images employed for the porosity measurements were acquired using a shielded JEOL 6400® scanning electron microscope equipped with a MaxView® software package from SAMx. Two-dimensional pore section areas and corresponding section diameters were measured, assuming that HBS pores are spherical [4,10,15]. It has been shown that the spherical pores in the HBS can

be very polydisperse [10,15]. In order to measure both small and large features, one possibility is to acquire images using different magnifications. From each image, only features within the appropriate size range are measured, and then the data from the different magnifications are combined [16].

On the same area, two magnifications were used: a low magnification of 500x with spatial resolution of ≈0.15 μm and a high magnification of 1500x with spatial resolution of ≈0.05 μm . The combination of the two magnifications increased the accuracy of the measurements and broadened the range of pore section diameters that could be measured. Each image was then processed using the software Image-Pro Analyzer® (v. 7.0, MediaCybernetics Inc., Rockville, MD, USA). In the first step of the QIA, a median filter was applied to reduce the Gaussian noise. Then a global thresholding mask was employed to threshold the image and separate the pore sections from the background. After the mask was created, the resolution limit was chosen to be 2.6 times the spatial resolution of the image, i.e. ≈0.39 μm for the images at 500x and ≈0.13 μm for the images at 1500x. All the pore section diameters smaller than the selected resolution limit were discarded. After that, the two pore section diameter distributions obtained from the images at different magnifications were merged. The cut-off section diameter was chosen in an interval where the two distributions are comparable, as shown in Fig. 1a).

All the pore sections from the distribution obtained at a magnification of 1500x with a section diameter above the cut-off threshold were removed. The same was done for the pore sections from the distribution at low magnification with a section diameter below the cut-off threshold, resulting in a final, merged distribution as reported in Fig. 1b). Only in a few cases the distributions obtained with the two magnifications were the same. In such cases, only images at lower magnification were used.

The total pore area is given by summing the areas of the measured pore sections after the merging. The areal porosity is calculated as the ratio between the total pore area and the image area.

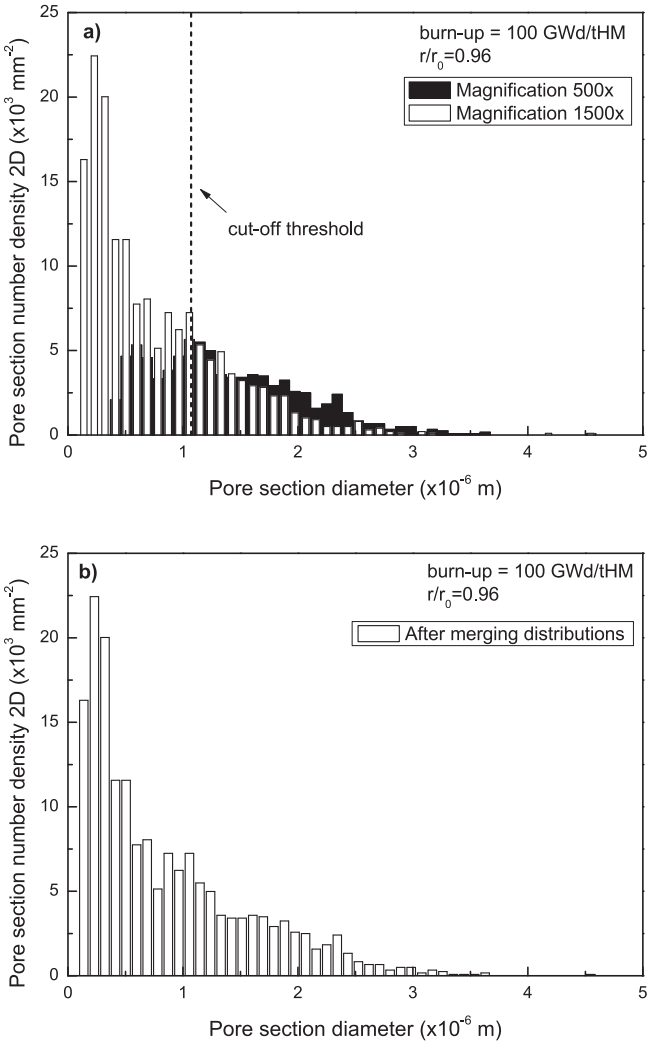

Fig. 1. a) Two-dimensional pore section diameter distributions obtained on the same area at the two magnifications before merging. b) Resulting two-dimensional pore section diameter distribution after merging the images at the two magnifications.

3. Results and discussion

3.1. Empirical study of the relation between microhardness and Young's modulus

Extensive studies have been performed about the relationship between hardness and Young's modulus, also in relation to other mechanical properties [17–20]. The related methodology is developed for instrumented indentation techniques and would have limited applicability to static indentation tests as the ones here performed. Firstly, in this work only the residual projected area of the hardness impression after load removal is measured, which might be different from the projected contact area during load application used in the instrumented indentation [21]. Secondly, no model specifically considers crack formation during the indentation tests, which were observed in some of our measurements (see Fig. 2). For the scope of the present work, the relationship between the measured microhardness and the Young's modulus was studied only empirically. The ratios between the measurements obtained from the Vickers microindentation tests and the acoustic microscopy at different values of local burn-up were calculated and are reported in Fig. 3. The ratio microhardness/elastic modulus ($HV_{0.1}/E$) is constant over a large range of burn-ups (60–112 GWd/tHM) and, hence, pore volume fractions (0.04–0.13), even when the HBS has formed (data points above 80 GWd/tHM in Fig. 3), with a mean value 0.057. The measured ratios are in good agreement also with previous measurements on other high burn-up UO_2 fuels [22].

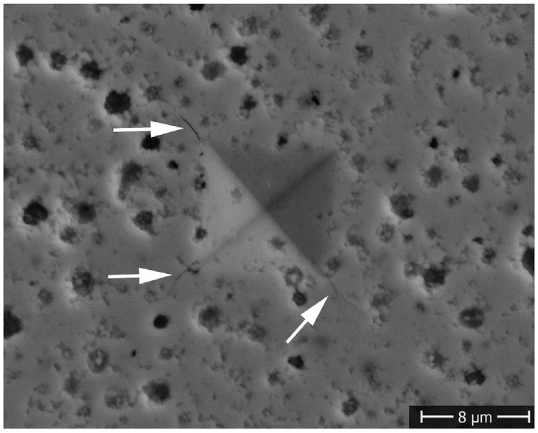

Fig. 2. Representative SEM-micrograph of fuel indentation imprint using 0.98 N load. White arrows point out the cracks sometimes observed at the imprint tips.

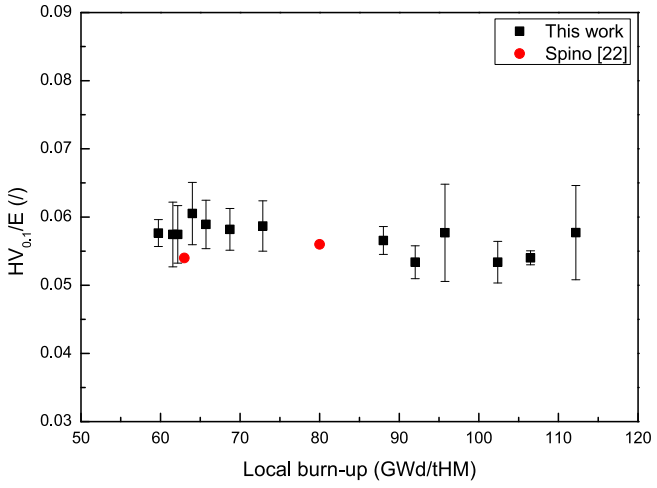

Fig. 3. Measured Vickers microhardness to Young's modulus ratio $HV_{0.1}/E$ as a function of the local burn-up. The results of the present work (black squares) are in good agreement with previous results (red circles) [22]. (For interpretation of the references to colour in this figure legend, the reader is referred to the web version of this article.)

3.2. Mechanical properties and local porosity

On the basis of the findings reported above and assuming that, as a first approximation, the porosity dependence of hardness should reflect that of the elastic moduli [4,23,24], we could use the measured microhardness as local probe for the variation of Young's modulus with local porosity in the HBS.

First, the relationship between the microhardness and the measured fuel local porosity had to be established. The results are reported in Fig. 4. Considering the scatter of the data, it is not straightforward to establish a trend between the microhardness and the porosity. To the authors' knowledge, there is a limited amount of models that study the dependence of microhardness on porosity in ceramics [23–25]. Spino et al. [4] used an exponential relationship to fit Vickers microhardness data of high burn-up UO_2. Their analysis was based on the minimum solid area approach [26,27]. In the relatively small range of porosity investigated and considering the experimental scatter, also a linear fit could be employed (Fig. 4). The goodness of fit values in the two cases, estimated on the basis of the adjusted R^2, are in fact very similar and equal to 0.71 for the linear fit and 0.73 for the exponential fit.

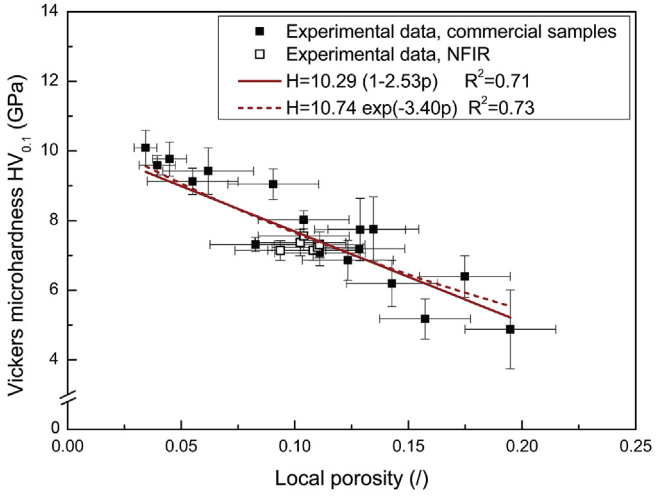

Fig. 4. Measured Vickers microhardness as a function of the local porosity. The error bars of the microhardness represent 95% confidence level. The error bars of the porosity represent the error in the porosity induced by the variation of the mask threshold.

Once established, the relationships were assumed to be Young's modulus dependence on porosity in irradiated UO_2 [4]. The assumption is corroborated by the constant ratio measured over a large range of porosity and burn-ups (see previous section).

The correlations obtained in Fig. 4 were compared to the relationships available in literature and implemented in various fuel performance codes. All these relationships are based on data from non-irradiated UO_2 [6,28–36]. The Young's modulus of stoichiometric UO_2 is generally expressed as follows [6,7,29].

$$E = E_0 f(p)\, g(T) \tag{4}$$

where E_0 (GPa) is the Young's modulus of the fully dense, non-irradiated UO_2 at room temperature, p (/) is the fractional porosity, T (°C) the temperature. Table 1 reports the values of several correlations available.

The experimental measurements performed in this study were conducted at room temperature. Therefore, the focus was only on the relationship with porosity.

Comparing the porosity correlations in Table 1 to the calculated linear relationship plotted in Fig. 4, no major differences are identifiable in the Young's modulus decrease with porosity between irradiated and non-irradiated UO_2. When taking into account the experimental uncertainties, the present set of data would not justify the introduction of another correlation to describe the decrease of Young's modulus with porosity in high burn-up irradiated UO_2, in particular in the HBS.

The present results do not confirm the findings in a previous work reported by Spino et al. [4], where the decreasing trend of Vickers microhardness in irradiated and non-irradiated fuel was found to be different. The reason of the different behaviour was explained in Ref. [4] in terms of pore shape. The pores in the HBS are spherical, whereas the intergranular pores outside the HBS have a more lenticular shape, thus contributing to a larger mechanical property decrease at a fixed value of porosity [4].

To evaluate the potential effect of the shape factor [37], a pore shape factor was calculated from the SEM images. The pore ellipse ratio, defined as the ratio between the major and the minor axes of the ellipse with equivalent area to the considered pore [38], was calculated. The majority of pore shape factors measured at various porosity remains fairly close to one, indicating the good approximation of the pore shape to a sphere (see Fig. 5). However, coarsened cavities (i.e. ellipse ratio > 2) are observed, with a frequency up to ≈5% (inset of Fig. 5). The pore-pore contact onset was also recognised for other similar samples [15,39]. This may explain a deviation from the behaviour observed by Spino et al. [4]. A similar explanation was given in Ref. [40] to explain deviation in the trend of the mechanical properties vs. porosity in HBS-analogue material compared to what was found in Ref. [4] for irradiated fuel.

Hence, on the basis of the present analysis, it is fair to conclude that the validity of the relationships $f(p)$ in Table 1 could be extended from non-irradiated to high burn-up UO_2 fuel, including

Table 1
Correlations of stoichiometric UO_2 Young's modulus available in literature.

E_0	$f(p)$	$g(T)$	Ref.
223.7	$1-2.6p$	$1-1.394\cdot10^{-4}(T-20)$	[6]
226	$1-2.62p$	$1-1.131\cdot10^{-4}T$	[7]
226.4	$1-2.752p$	$1-1.125\cdot10^{-4}T$	[8]
222.46	$1-2.5p$	$1-8.428\cdot10^{-5}T-4.381\cdot10^{-8}T^2$	[34]
220	$1-2.34p$	not reported	[35]

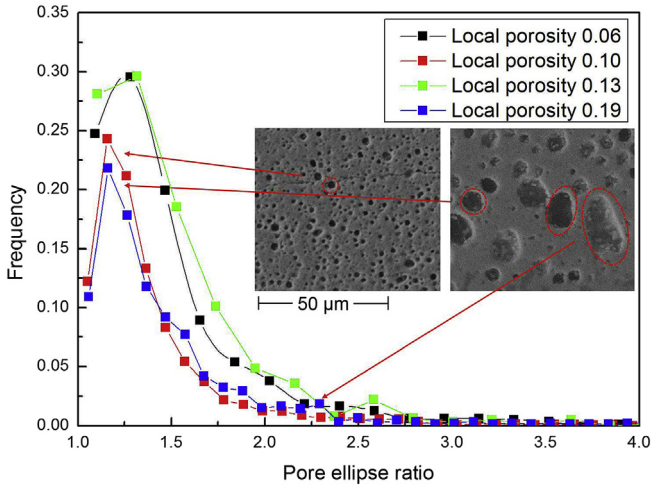

Fig. 5. Frequency distributions of the pore ellipse ratios for various level of local porosity. Pore ellipse ratios in the range 1–1.5 (corresponding to almost spherical pores) represent the majority of pore population. Coarsened pores (pore ellipse ratio >2) are also present (see inset in the Figure).

the HBS.

From the microhardness data as a function of local porosity (Fig. 4), the Young's modulus was calculated using the measured mean ratio $HV_{0.1}/E$ (section 3.1). The calculated results are reported in Fig. 6 together with the available data from acoustic microscopy both from this work and from the High Burnup Rim Project (HBRP) results [5].

The correlation currently implemented in TRANSURANUS V1M1J14 [6] and the MATPRO correlation [8], both evaluated at room temperature, are also plotted in Fig. 6 (dashed and dotted line, respectively). They generally overpredict the value of the Young's modulus of irradiated UO_2 at each value of porosity. The same conclusion is valid for the other correlations in Table 1, which are not included in the figure for clarity. Within the range of

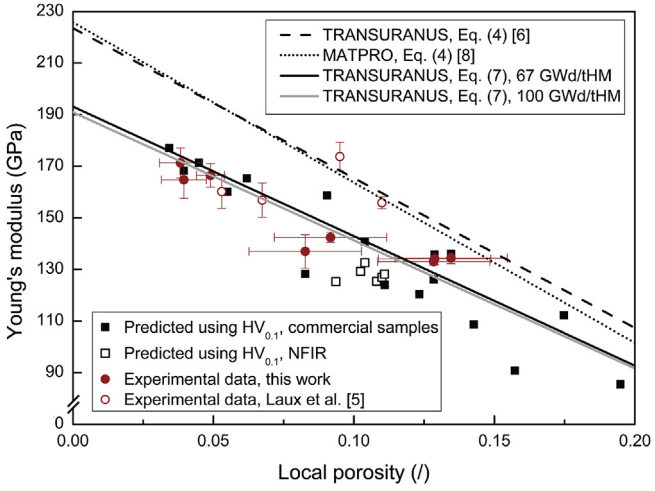

Fig. 6. Young's modulus as a function of local porosity and comparison to correlations used in fuel performance codes. Black and white squares: values predicted using Vickers microhardness data and the measured ratio $HV_{0.1}/E$. Red circles: data from acoustic microscopy in this work. White circles: data from literature [5]. Dashed black line: TRANSURANUS V1M1J14 correlation currently available [6]. Dotted black line: MATPRO correlation [8]. Solid black and grey lines: TRANSURANUS correlation implemented in this work for two values of local burn-up. (For interpretation of the references to colour in this figure legend, the reader is referred to the web version of this article.)

porosity analysed, the difference between the correlations presently available in literature (see Table 1) and the trend of the measured data is between 5% and 15%. The discrepancy is attributed to a burn-up accumulation effect, in agreement with a previous investigation [13,41].

Therefore, a modified relationship for the Young's modulus has been introduced (black and grey solid line in Fig. 6). An additional factor that takes into account the "apparent softening" due to burn-up was included, based on the experimental results reported by Laux et al. [5,41]. The new expression of E (GPa) is then given by

$$E = E_0\, f(p)\, g(T)\, h(bu) \tag{5}$$

where E_0, $f(p)$, and $g(T)$ have the same meaning as before and bu (GWd/tHM) is the local burn-up. The new factor introduced is

$$h(bu) = 1 - 0.1506\,[1 - \exp(-0.035\,bu)] \tag{6}$$

To summarise, the new correlation that will be available in the future version of TRANSURANUS is

$$E = 223.7(1 - 2.6\,p)\left[1 - 1.394\cdot 10^{-4}(T - 20)\right]\{1 - 0.1506\,[1 - \exp(-0.035\,bu)]\} \tag{7}$$

The new correlation of the Young's modulus (Eq. (7)) is in better agreement both with the experimental data and the predicted E using the microhardness measurements when compared to Eq. (4).

4. Integral fuel rod analyses

Following the introduction of Eq. (7), a pioneering work to illustrate its potential impact on the fuel rod performance calculations was undertaken. As first applications, we selected two cases of experimental rods irradiated up to high burn-up from the OECD/NEA International Fuel Performance Experiments (IFPE) database [42]:

- JAERI pulse-irradiation test FK-1, involving base irradiation up to ≈45 GWd/tHM, re-fabrication, and pulse-irradiation at cold startup in the NSRR (Japan).
- Halden Reactor Project IFA-597.3 rod 8, involving base irradiation up to ≈68 GWd/tHM, re-fabrication, and transient test in the Halden HWR (Norway).

Considering the high burn-up of these rods, the experiments are valuable for evaluating the impact of the fuel Young's modulus correlation (see Eq. (7) in section 3.2) on pellet-cladding mechanical interaction (PCMI) and fuel pin deformation at high burn-up. The PCMI and pin deformations are determined by the thermo-mechanical properties of both fuel and cladding. In this preliminary assessment however, we hereby focus only on fuel properties. The main models and characteristics of the TRANSURANUS code are summarised in Refs. [43–47]. The mechanical analysis is treated in a quasi two-dimensional approach, based on three main assumptions: (a) a generalised plane-strain condition is valid in the axial direction, (b) the fuel rod is considered axisymmetric, and (c) the fuel and cladding elastic constants are locally isotropic and constant [45,48].

Among the various thermophysical properties involved in the fuel performance calculations, the fuel thermal conductivity has particular relevance [49,50]. In this work, the standard correlation implemented in TRANSURANUS was employed [50]. The degradation of the thermal conductivity with burn-up is based on the data of thermal diffusivity of high burn-up UO_2 from Ronchi et al. [51],

but does not account for the potential recovery of the lattice thermal conductivity in the HBS [51–53]. A more comprehensive correlation that would consider the potential recovery of the lattice thermal conductivity will be considered in the future.

4.1. Case FK-1

This case allowed illustrating the impact of the new burn-up-dependent term introduced in Eq. (7) under extreme conditions, namely a reactivity-initiated-accident (RIA) that has also been analysed in the frame of the FUMEX-III benchmark organised by the IAEA [54]. The simulation was run once using Eq. (4) [6] and once using the new Eq. (7). To model the PCMI, the URFRIC model [47] was used. More details of the calculation can be found in Ref. [54].

The results of the FK-1 case for illustrating the impact of the new correlation for the Young's modulus are reported in Figs. 7 and 8. The available experimental measurements [55,56] and the pulse time profile [54] are also reported on the graphs. In both figures, the solid line is the result of the simulations using Eq. (4) [6], whereas the dashed line is the result employing Eq. (7). Before the pulse irradiation, no bonding was observed between the fuel and the cladding [56], which is well reproduced by the fuel performance code (Fig. 7). Under the hypotheses of the mechanical models employed [44,47], the calculations indicate a small variation of the gap width due to the increased fuel softening (Fig. 7). The fuel stack elongation variation is ≈3% (Fig. 8). The slight decrease observed would suggest that the fuel stack elongation is restrained by the prolonged contact with the cladding tube (Fig. 7). However, it is not straightforward to interpret the results, due to the obvious differences between the predicted and measured kinetics in this type of transients (Fig. 8) [54]. Nevertheless, what seems to emerge from the calculation output is that the fuel Young's modulus softening at high burn-up has a small impact on the overall calculated results even under such extreme conditions.

4.2. IFA-597.3

As in the previous case, the simulations were run once using Eq. (4) [6] and once using the new Eq. (7). In this case, a pure 'no-slip' model between cladding and fuel was assumed [44]. More details can be found in the final report of the FUMEX-II benchmark organised by the IAEA [57].

Two relevant results of the TRANSURANUS simulations are reported in Figs. 9 and 10. They show the calculated cladding elongation (Fig. 9) and the cladding outer radius (Fig. 10) during the final transient test. The linear heat rate is plotted [57] on the lower part of the figures. In each figure, the results of the simulations in the two different cases are compared.

As can be seen from Figs. 9 and 10, also in this simulation the additional softening of the fuel Young's modulus reduces the cladding axial and radial deformation by a limited amount. The accuracy of the present results is inevitably limited by the knowledge of the fuel and cladding properties at high burn-up, and high burn-up-related phenomena for which a comprehensive model is still lacking (e.g., fission gas release from the HBS or pellet-cladding bonding). However, it is useful to provide a first evaluation of the effects of the updated fuel Young's modulus expression on the

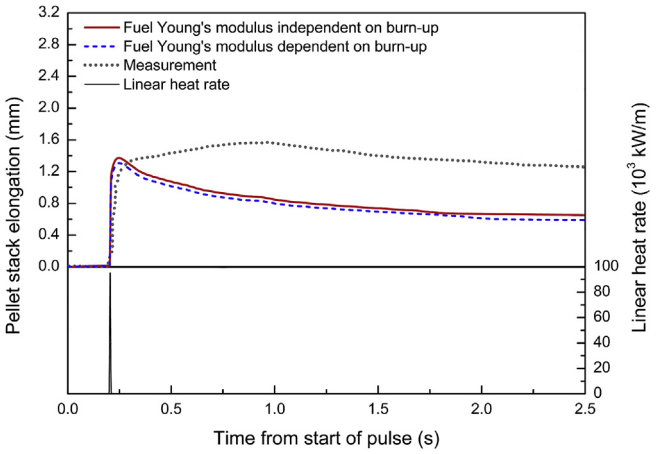

Fig. 8. Pellet stack elongation of rod FK-1 during the first 2.5 s after the pulse test initiation. In the lower part of the graph the pulse time profile is reported [54] (pulse width: 4.4 ms). In the upper part, two calculations of the pellet stack elongation are shown changing the fuel Young's modulus, one employing Eq. (4) [6] (red solid curve) and one employing Eq. (7) (blue dashed curve). For comparison, also the measurement results are reported [55,56] (grey dotted curve). (For interpretation of the references to colour in this figure legend, the reader is referred to the web version of this article.)

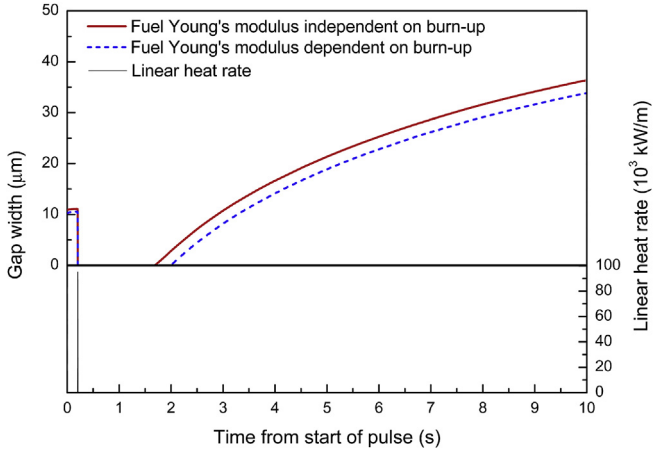

Fig. 7. Calculations of the gap width of rod FK-1 during the first 10 s after the pulse test initiation. In the lower part of the graph the pulse time profile is reported [54] (pulse width: 4.4 ms). In the upper part, two calculations of the gap width are shown changing the fuel Young's modulus, one employing Eq. (4) [6] (red solid curve) and one employing Eq. (7) (blue dashed curve). (For interpretation of the references to colour in this figure legend, the reader is referred to the web version of this article.)

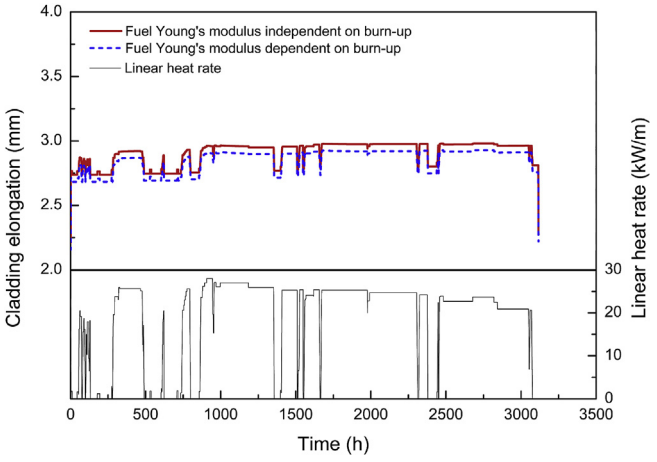

Fig. 9. Cladding elongation of IFA-597.3 rod 8 during the final transient test. In the lower part of the graph the time profile of the linear power rate is reported [57]. The calculations were performed changing the fuel Young's modulus only, once employing Eq. (4) [6] (red solid curve) and once employing Eq. (7) (blue dashed curve). (For interpretation of the references to colour in this figure legend, the reader is referred to the web version of this article.)

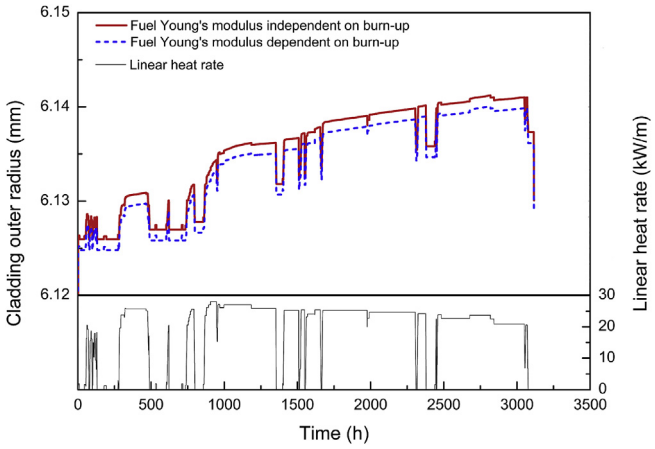

Fig. 10. Cladding outer radius of IFA-597.3 rod 8 during the final transient test. In the lower part of the graph the time profile of the linear power rate is reported [57]. The calculations were performed changing the fuel Young's modulus only, once employing Eq. (4) [6] (red solid curve) and once employing Eq. (7) (blue dashed curve). (For interpretation of the references to colour in this figure legend, the reader is referred to the web version of this article.)

integral fuel performance. In both cases analysed, the burn-up dependent softening factor had a small impact on the simulation results. Further analyses on a more comprehensive set of cases are advisable in order to ascertain these first observations.

5. Conclusions

The Young's modulus dependence on porosity in high burn-up fuel, in particular in the HBS, has been evaluated exploiting the synergy between two experimental post-irradiation examination techniques, i.e., Vickers microindentation and acoustic microscopy. The present data, in combination with Young's modulus data of irradiated UO_2 available in literature, were used for the first time to introduce a new correlation for the Young's modulus of irradiated UO_2 fuel that will be available in the future in the fuel performance code TRANSURANUS.

Concerning the porosity dependence, the linear relation established using the present experimental data is found to be close to the correlation currently implemented in TRANSURANUS [6]. A burn-up dependent term has been introduced in the expression of the Young's modulus, based on previous measurements conducted on high burn-up fuel [5,41]. The range of experimental validation of the TRANSURANUS correlation of the fuel Young's modulus is thus extended from non-irradiated to irradiated UO_2 fuel and for porosity up to 20%.

The availability of the herein developed correlation for the fuel Young's modulus allowed to illustrate the impact of the additional fuel softening at high burn-up on PCMI. For this purpose, we have performed code simulations of two experimental rods at high burn-up from the IFPE database that cover operational transient as well as design-basis accidents (DBA) conditions (i.e., RIA).

The outcome of these first simulations indicates that for the specific cases here considered the fuel Young's modulus variation at high burn-up (i.e., the reduction of the Young's modulus caused by an increase in burn-up) has limited impact on the calculated outputs. Nevertheless, further simulations are required in order to verify whether these observations are also hold in other cases.

Acknowledgements

The authors are indebted to G. Paperini, R. Gretter and R. Nasyrow (JRC-ITU) for the sample preparation, and to D. Pellottiero (JRC-ITU) for his help in the acquisition of the SEM images. Special thanks are conveyed to G. Despaux, D. Laux (IES-University of Montpellier), and L. Fongaro (JRC-ITU) for their scientific advice. The authors are thankful to AREVA GmbH for providing some of the commercial samples. We also acknowledge the NFIR project and thank its members for the permission to publish the results obtained on the special irradiation discs. This work was financially supported by the European Commission through the Training and Mobility of Researchers program and the GENTLE project (Grant Agreement 198236) in the 7th Framework Program and Horizon 2020 of the European Commission.

References

[1] B. Michel, J. Sercombe, C. Nonon, O. Fandeur, 3.22-Modeling of pellet cladding interaction, in: R.J.M. Konings (Ed.), Comprehensive Nuclear Materials, Elsevier, 2012.
[2] B. Baurens, J. Sercombe, C. Riglet-Martial, L. Desgranges, L. Trotignon, P. Maugis, 3D thermo-chemical-mechanical simulation of power ramps with ALCYONE fuel code, J. Nucl. Mater 452 (2014) 578–594.
[3] P. Van Uffelen, M. Sheindlin, V. Rondinella, C. Ronchi, On the relations between the fission gas behaviour and the pellet-cladding mechanical interaction in LWR fuel rods, in: Pellet-Clad Interaction in Water Reactor Fuels, 2004. Aix-en-Provence, France.
[4] J. Spino, J. Cobos-Sabate, F. Rousseau, Room-temperature microindentation behaviour of LWR-fuels, part 1: fuel microhardness, J. Nucl. Mater. 322 (2003) 204–216.
[5] D. Laux, D. Baron, G. Despaux, A. Kellerbauer, M. Kinoshita, Determination of high burn-up nuclear fuel elastic properties with acoustic microscopy, J. Nucl. Mater. 420 (2012) 94–100.
[6] K. Lassmann, A. Moreno, The light-water-reactor version of the URANUS integral fuel-rod code, Tech. rep., Institute of Reactor Technology, Technical University of Darmstadt, 1977.
[7] P. MacDonald, L. Thompson, MATPRO – Version 09. A Handbook of Material Properties for the Use in the Analysis of Light Water Reactor Fuel Rod Behavior, TREE-NUREG-1005, Idaho National Engineering Lab., Idaho Falls (USA), 1976.
[8] D.L. Hagrman, G.A. Reymann, MATPRO – Version 11. A Handbook of Material Properties for the Use in the Analysis of Light Water Reactor Fuel Rod Behavior, NUREG/CR-0497 TREE-1280 R3, Idaho National Engineering Lab., Idaho Falls (USA), 1979.
[9] E.A. Dean, Elastic moduli of porous sintered materials as modeled by variable-aspect-ratio self-consistent oblate-spheroidal-inclusion theory, J. Amer. Ceram. Soc. 66 (1983) 847–854.
[10] J. Spino, K. Vennix, M. Coquerelle, Detailed characterisation of the rim microstructure in PWR fuels in the burn-up range 40-67 GWd/tHM, J. Nucl. Mater. 231 (1996) 179–190.
[11] S.K. Yagnik, T. Tverberg, E. Kolstad, J.A. Turnbull, D. Baron, M. Kinoshita, Fuel (UO_2) R&D: needs, approaches and results, in: Water Reactor Fuel Performance Meeting, 2008. Seoul, Republic of Korea.
[12] ASTM, Standard Test Method for Vickers Indentation Hardness of Advanced Ceramics, 1999, pp. C 1327–1399. Copyright© ASTM.
[13] D. Laux, Caractérisation mécanique de combustibles nucléaires à fort taux de combustion par méthodes micro-acoustiques, University Montpellier II, 2002. Ph.D. thesis.
[14] D. Laux, W. de Weerd, D. Papaioannou, S. Kitajima, V. Rondinella, G. Despaux, Scanning acoustic microscope for mechanical characterization and density estimation of irradiated nuclear fuel, Prog. Nucl. Energ. 72 (2014) 63–66.
[15] J. Spino, A. Stalios, H. Santa Cruz, D. Baron, Stereological evolution of the rim structure in PWR-fuels at prolongated irradiation: dependencies with burn-up and temperature, J. Nucl. Mater. 354 (2006) 66–84.
[16] J. Russ, Image Analysis of Food Microstructure, CRC Press, Boca Raton, Florida, USA, 2005, pp. 306–308.
[17] W. Oliver, G. Pharr, An improved technique for determining hardness and elastic modulus using load and displacement sensing indentation experiments, J. Mater. Res. 7 (1992) 1564–1583.
[18] W. Oliver, G. Pharr, Measurement of hardness and elastic modulus by instrumented indentation: advances in understanding and refinements to methodology, J. Mater. Res. 19 (2004) 3–20.
[19] Y.-T. Cheng, C.-M. Cheng, Scaling, dimensional analysis, and indentation measurements, Mater. Sci. Eng. R. 44 (2004) 91–149.
[20] A. Giannakopoulos, P.-L. Larsson, R. Vestegaard, Analysis of Vickers indentation, Int. J. Solids Struct. 31 (1994) 2679–2708.
[21] Z. Li, Y.-T. Cheng, H.T. Yang, S. Chandrasekar, On two indentation hardness definitions, Surf. Coat. Tech. 154 (23) (2002) 124–130.
[22] J. Spino, Determination of the Young's Modulus of Irradiated Fuels by Knoop Indentation, European Commission, JRC-ITU, 2005. Annual Activity Report.
[23] R. Rice, Ch. 6 – Hardness and related properties, in: *Porosity of Ceramics*, Marcel Dekker Inc., 1998, pp. 276–291.

[24] J. Luo, R. Stevens, Porosity-dependence of elastic moduli and hardness of 3Y-TZP ceramics, Ceram. Int. 25 (1999) 281–286.
[25] P. Arató, E. Besenyei, A. Kele, F. Wéber, Mechanical properties in the initial stage of sintering, J. Mater. Sci. 30 (1995) 1863–1871.
[26] R. Rice, Evaluation and extension of physical property-porosity models based on minimum solid area, J. Mater. Sci. 31 (1996) 102–118.
[27] R. Rice, Ch. 2 – Evaluation of porosity dependence of properties, in: *Porosity of Ceramics*, Marcel Dekker Inc., 1998, pp. 72–84.
[28] H. Stehle, H. Assmann, F. Wunderlich, Uranium dioxide properties for LWR fuel rods, Nucl. Eng. Des. 33 (1975) 230–260.
[29] H. Többe, Der Brennstab-Code IAMBUS, Technischer Bericht 73.65, Interatom, 1973.
[30] J. Hales, R.L. Williamson, S. Novascone, G. Pastore, B. Spencer, D. Stafford, K. Gamble, D. Perez, W. Liu, BISON Theory Manual - The Equations behind Nuclear Fuel Analysis, INL/EXT-13–29930, 2014. Idaho Falls, (USA).
[31] M. Suzuki, H. Saitou, Y. Udagawa, F. Nagase, Light Water Reactor Fuel Analysis Code FEMAXI-7. Model and Structure, Copyright © 2013, JAEA-Data/Code 2013-005, Reactor Safety Research Unit, Nuclear Safety Research Center, Japan Atomic Energy Agency, 2013.
[32] Fuel Performance Analysis Capability in FALCON, 1002866, EPRI, Palo Alto, CA, 2002.
[33] K. Geelhood, W. Luscher, P. Raynaud, I. Porter, FRAPCON-4.0: A Computer Code for the Calculation of Steady-State, Thermal-Mechanical Behavior of Oxide Fuel Rods for High Burnup, PNNL-19418, Vol. 1, Pacific Northwest National Laboratory, Richland, Washington, 2015. Rev.2.
[34] D. Martin, The Elastic Constants of Polycrystalline UO_2 and (U,Pu) Mixed Oxides: a Review and Recommendations 21, High Temp.-High Press, 1989, pp. 13–24.
[35] J. Boocock, A. Furzer, J. Matthews, The Effect of Porosity on the Elastic Moduli of UO_2 as Measured by an Ultrasonic Technique, AERE-M 2565, UK Atomic Energy Authority, 1972.
[36] SCDAP/RELAP5-3D©Code development team, SCDAP/RELAP5-3D©CODE MANUAL. MATPRO - A Library of Material Properties for Light-water-reactor Accident Analysis, INEEL/EXT-02-00589, Idaho National Engineering Lab., Idaho Falls (USA), 2003.
[37] J.C. Russ, 8-Image measurements, in: The Image Processing Handbook, CRC Press, 1998.
[38] A.I. Medalia, Dynamic shape factors of particles, Powder Technol. 4 (3) (1971) 117–138.
[39] A. Romano, M.I. Horvath, R. Restani, Evolution of porosity in the high-burnup fuel structure, J. Nucl. Mater. 361 (2007) 62–68.
[40] J. Spino, H. Santa Cruz, R. Jovani-Abril, R. Birtcher, C. Ferrero, Bulk-nano-crystalline oxide nuclear fuels – an innovative material option for increasing fission gas retention, plasticity and radiation-tolerance, J. Nucl. Mater. 422 (2012) 27–44.
[41] D. Laux, G. Despaux, F. Augereau, J. Attal, D. Baron, J. Gatt, V. Basini, P.M. Chantoin, J.-M. Saurel, Ultrasonic measurement of high burn-up fuel elastic properties, in: 6th International Conference on WWER Fuel Performance, Modelling and Experimental Support, Albena, Bulgaria, 2005.
[42] E. Sartori, J. Killeen, J. Turnbull, International Fuel Performance Experiments (IFPE) Database, OECD/NEA, 2010. http://www.oecd-nea.org/science/fuel/ifpelst.html.
[43] K. Lassmann, TRANSURANUS: a fuel rod analysis code ready for use, J. Nucl. Mater 188 (1992) 295–302.
[44] K. Lassmann, H. Blank, Modelling of fuel rod behaviour and recent advances of the TRANSURANUS code, Nucl. Eng. Des. 106 (1988) 291–313.
[45] K. Lassmann, URANUS – a computer programme for the thermal and mechanical analysis of the fuel rods in a nuclear reactor, Nucl. Eng. Des. 45 (1978) 325–342.
[46] K. Lassmann, An iterative model for calculating the crack structure in fuel-rod design, in: 4th International Conference on Structural Mechanics in Reactor Technology, 1977. Transactions Vol. C, Paper C 1/3, San Francisco, United States.
[47] K. Lassmann, Treatment of axial friction forces in the TRANSURANUS code, Eur 13660 en, Commission of the European Communities, 1991.
[48] V. Di Marcello, A. Schubert, J. van de Laar, P. Van Uffelen, The TRANSURANUS mechanical model for large strain analysis, Nucl. Eng. Des. 276 (2014) 19–29.
[49] S.K. Yagnik, Thermal conductivity recovery phenomenon in irradiated UO_2 and (U, Gd)O_2, in: Water Reactor Fuel Performance Meeting, 2000. Park City, Utah.
[50] K. Lassmann, A. Schubert, J. van de Laar, C. Vennix, Recent developments of the TRANSURANUS code with emphasis on high burnup phenomena, in: Proceedings of a Technical Committee Meeting on Nuclear Fuel Behaviour Modelling at High Burnup and its Experimental Support, 2000. Windermere, United Kingdom.
[51] C. Ronchi, M. Sheindlin, D. Staicu, M. Kinoshita, Effect of burn-up on the thermal conductivity of uranium dioxide up to 100.000 $MWdt^{-1}$, J. Nucl. Mater. 327 (2004) 58–76.
[52] D. Staicu, 2.17-Thermal properties of irradiated UO_2 and MOX, in: R.J. Konings (Ed.), Comprehensive Nuclear Materials, Elsevier, 2012.
[53] X.-M. Bai, M.R. Tonks, Y. Zhang, J.D. Hales, Multiscale modeling of thermal conductivity of high burnup structures in UO_2 fuels, J. Nucl. Mater 470 (2016) 208–215.
[54] International Atomic Energy Agency, Improvement of Computer Codes Used for Fuel Behaviour Simulation (FUMEX-III), IAEA-TECDOC-1697, IAEA, 2013.
[55] T. Nakamura, M. Yoshinaga, M. Takahashi, K. Okonogi, K. Ishijima, Boiling water reactor fuel behavior under reactivity-initiated-accident conditions at burnup of 41 to 45 GWd/tonne U, Nucl. Technol. 129 (2000) 141–151.
[56] T. Fuketa, T. Nakamura, H. Sasajima, F. Nagase, H. Uetsuka, K. Kikuchi, T. Abe, Behavior of PWR and BWR fuels during reactivity-initiated accident conditions, in: Water Reactor Fuel Performance Meeting, Park City, Utah, 2000.
[57] International Atomic Energy Agency, Fuel Modelling at Extended Burnup (FUMEX-II), IAEA-TECDOC-1687, IAEA, 2012.